condensed matter

MDPI

Article

The Transport and Optical Characteristics of a Metal Exposed to High-Density Energy Fluxes in Compressed and Expanded States of Matter

Nikolay B. Volkov and Alexander I. Lipchak *

Institute of Electrophysics of the Ural Branch of the Russian Academy of Sciences, 106, Amundsen St., 620016 Yekaterinburg, Russia; admin@iep.uran.ru
* Correspondence: lipchak@iep.uran.ru

Abstract: This article presents a theoretical study of the optical and transport properties of metals. Iron, as an example, was used to discuss, through a theoretical description, the peculiarities of these properties in the compressed and expanded states under the influence of high-density energy fluxes. By solving the semi-classical Boltzmann equation for conduction electrons for a broad range of densities and temperatures, the expressions of electrical conductivity, electronic thermal conductivity, and thermoelectric coefficient calculations were derived. The real and imaginary parts of the iron permittivity and the energy absorption coefficient for the first and second harmonics of Nd:YAG laser radiation were obtained. The calculation peculiarities of the metal's optical characteristics of matter in an expanded state in a broad range of densities and temperatures were considered. The analysis of the obtained results shows their agreement with the theoretical description for cases of ideal non-degenerate and dense degenerate electron plasmas. It is shown that the behavior of the electrical conductivity and optical characteristics in the critical and supercritical regions of density and temperature are in agreement with the known experimental results.

Keywords: transport and optical characteristics of metals; high-density energy flux; long-wave structure factor; liquid–vapor and metal–insulator phase transitions; behavior of transport and optical characteristics in the critical point region

Citation: Volkov, N.B.; Lipchak, A.I. The Transport and Optical Characteristics of a Metal Exposed to High-Density Energy Fluxes in Compressed and Expanded States of Matter. *Condens. Matter* **2023**, *8*, 70. https://doi.org/10.3390/condmat8030070

Academic Editors: Viorel-Puiu Paun, Eugen Radu, Maricel Agop and Mircea Olteanu

Received: 22 June 2023
Revised: 31 July 2023
Accepted: 31 July 2023
Published: 11 August 2023

1. Introduction

This paper presents the development of our initially proposed and published model [1]. The peculiarities of the theoretical description of the thermodynamic properties of a metal accounting for the phase transitions (PTs) of metal–liquid, liquid–gas, and metal–insulator occurring within a wide range of densities and temperatures are studied. The study of electronic transport and optical properties is the main objective of this paper. The non-equilibrium properties of matter in various aggregate states are studied within the framework of the classical kinetic theory formulated in the works of J.K. Maxwell [2], L. Boltzmann [3], and G.A. Lorenz [4], which is still in active development. Since these works were published, the number of papers has increased, and the field of knowledge has expanded so much that we must apologize to those investigators whose papers we do not mention. The current state of the methods of theoretical study for these properties of matter is shown well for condensed matter in [5–12] and for dense gases and non-ideal plasma in [13–20]. A distinctive trend of modern theoretical research is the development of ab initio computer techniques for transport and optical property calculations, e.g., [9–12,17–20] and the references therein. Despite tremendous progress in computer technology and calculation speed growth, these methods still require considerable computer resources to obtain significant results. Hence, these techniques do not cancel out the theoretical–analytical approach. Therefore, in the proposed work, we study the properties of a metal based on the solution of the semi-classical Boltzmann kinetic equation for conduction

electrons, written in reference to a quasi-neutral atomic cell [21]. We used well-known analytical methods (see [21–25] and the references therein) to find the solution to this equation. Considerable attention was paid to determining the mean free path of electrons and considering its relationship with the thermophysical properties of the metal in our earlier works [21,22,24]. The unique quality of our approach, as outlined in our previous article [1], is the joint description of the thermal and electrical processes occurring in the expanded and compressed metal. The metal model proposed in this paper makes it possible to determine thermodynamic functions while accounting for the PTs. The model has limitations in accounting for PTs' influence on the expanded state alone. The effect of structure and PTs during compression require a separate study.

2. Results

2.1. Transport Properties of Metal in a Quasi-Stationary Electromagnetic Field

Here, we use the known plasma model of a metal [22,24,26] for the calculation of the electronic kinetic coefficients in a compressed and expanded state, i.e., we consider the metal to be a plasma-like medium with a symmetric part of the distribution function of the conduction electrons conforming to Fermi–Dirac statistics [27]. One can write the generalized Ohm and Fourier laws in the center of the mass reference frame of a quasi-neutral atomic cell [21] as follows [24,28]:

$$\mathbf{E} + \frac{1}{e}\nabla\mu_1 = \frac{1}{M_{00}}\mathbf{j} + \alpha\nabla T; \tag{1}$$

$$\mathbf{q} = \frac{\mu_1 K_{00} - eK_{01}}{\mu_1 M_{00} - eM_{01}}\alpha T\mathbf{j} - \frac{\mu_1}{e}\mathbf{j} - \kappa\nabla T. \tag{2}$$

Here, $\mathbf{E}$ is the electric field, $\mathbf{j}$ is the current density, $\mathbf{q}$ is the density of the electron heat flow, $\mu_1(V_a,T)$ is the chemical potential of the conduction electrons (see [1] and the references therein), and $\alpha(V_a,T)$ is the thermoelectric coefficient, defined as follows:

$$\alpha = \frac{1}{eT}\left(\mu_1 - \frac{eM_{01}}{M_{00}}\right) \tag{3}$$

The electronic thermal conductivity $\kappa(V_a,T)$ is defined as follows:

$$\kappa = \frac{K_{00}}{eT}\left(\frac{M_{01}}{M_{00}}\left(\mu_1 - \frac{eK_{01}}{K_{00}}\right) - \frac{K_{01}}{K_{00}}\left(\mu_1 - \frac{eK_{02}}{K_{01}}\right)\right) \tag{4}$$

$M_{oi}(V_a,T)$ and $K_{oi}(V_a,T)$, i = 0, 1, 2, are the Onsager kinetic coefficients, and e, V_a, and T are the electron charge, the volume of an atomic cell, and the temperature, respectively.

Using well-known analytical methods [21–25], one can obtain expressions for the Onsager coefficients by solving the semi-classical Boltzmann equation for conduction electrons. In the SGS system, they will be as follows:

$$\begin{aligned} M_{0\beta} &= \tfrac{2me^{2-\beta}}{3\pi^2\hbar^3}\tfrac{\partial}{\partial\mu_1}\int_0^\infty \varepsilon^{\beta+1} l_{j,eff}(\varepsilon)(\exp((\varepsilon-\mu_1)/T)+1)^{-1}d\varepsilon = \\ &= \tfrac{2}{3\pi^2 e^\beta\hbar}\left(\tfrac{me^4}{\hbar^2}\right)^{\beta+1}\overline{T}^{\beta+1}\tfrac{\partial}{\partial x}\int_0^\infty \xi^{\beta+1}\bar{l}_{j,eff}(\xi)f_0(\xi-x)d\xi = \\ &= \tfrac{1}{e^\beta\hbar}E_H{}^{\beta+1}\overline{M}_{0\beta},\ \beta = 0,1,2; E_H = \tfrac{me^4}{\hbar^2}, \xi = \tfrac{\varepsilon}{T} = \tfrac{\bar{\varepsilon}}{\overline{T}}, \\ &x = \tfrac{\mu_1}{T} = \tfrac{\overline{\mu}_1}{\overline{T}}, \overline{T} = \tfrac{T}{E_H}, \overline{\mu}_1 = \tfrac{\mu_1}{E_H}, \bar{l}_{j,eff} = \tfrac{l_{j,eff}}{a_B}, a_B = \tfrac{\hbar^2}{me^2}; \end{aligned} \tag{5}$$

$$\begin{aligned} K_{0\beta} &= \tfrac{2me^{2-\beta}}{3\pi^2\hbar^3}\tfrac{\partial}{\partial\mu_1}\int_0^\infty \varepsilon^{\beta+1} l_{q,eff}(\varepsilon)(\exp((\varepsilon-\mu_1)/T)+1)^{-1}d\varepsilon = \\ &= \tfrac{2}{3\pi^2 e^\beta\hbar}\left(\tfrac{me^4}{\hbar^2}\right)^{\beta+1}\overline{T}^{\beta+1}\tfrac{\partial}{\partial x}\int_0^\infty \xi^{\beta+1}\bar{l}_{q,eff}(\xi)f_0(\xi-x)d\xi = \\ &= \tfrac{1}{e^\beta\hbar}E_H{}^{\beta+1}\overline{K}_{0\beta},\ \ \beta = 0,1,2; \bar{l}_{q,eff} = \tfrac{l_{q,eff}}{a_B}. \end{aligned} \tag{6}$$

Here, in relation to (5) and (6),

$$\begin{aligned} \overline{M}_{0\beta} &= \tfrac{2}{3\pi^2}\overline{T}^{\beta+1}\tfrac{\partial}{\partial x}\int_0^\infty \xi^{\beta+1}\bar{l}_{j,eff}(\xi)f_0(\xi-x)d\xi,\ \beta=0,1,2; \\ \overline{K}_{0\beta} &= \tfrac{2}{3\pi^2}\overline{T}^{\beta+1}\tfrac{\partial}{\partial x}\int_0^\infty \xi^{\beta+1}\bar{l}_{q,eff}(\xi)f_0(\xi-x)d\xi,\ \beta=0,1,2; \end{aligned} \tag{7}$$

$E_H = me^4\hbar^{-2}$ and $a_B = \hbar^2/(me^2)$ are the Hartree energy and the Bohr radius. Also, $l_{j,eff}(\varepsilon)$ and $l_{q,eff}(\varepsilon)$ are the electrons' mean free paths responsible for an electric current and a heat transfer in a matter. These values are represented in the system of atomic units (SAU) [29]. Table A1 of Appendix A provides brief information about this system that is necessary for understanding it. Using the normalization condition of the Fermi–Dirac function (see expression (29) in [1]), one can represent relation (7) as follows:

$$\begin{aligned} \overline{M}_{0\beta} &= \tfrac{\sqrt{2}z_i\overline{n}_i\overline{T}^{\beta-1/2}}{3}\tfrac{\frac{\partial}{\partial x}\int_0^\infty \xi^{\beta+1}\bar{l}_{j,eff}(\xi)f_0(\xi-x)d\xi}{F_{1/2}(x)}, \\ \overline{K}_{0\beta} &= \tfrac{\sqrt{2}z_i\overline{n}_i\overline{T}^{\beta-1/2}}{3}\tfrac{\frac{\partial}{\partial x}\int_0^\infty \xi^{\beta+1}\bar{l}_{q,eff}(\xi)f_0(\xi-x)d\xi}{F_{1/2}(x)}, \overline{n}_i = \tfrac{{a_B}^3}{V_a} = 1/\overline{V}_a. \end{aligned} \tag{8}$$

Here, z_i is the number of conduction electrons per atomic cell or the average ion charge, and $z_i\overline{n}_i$ is their concentration. $F_\nu(x) = \int_0^\infty (\exp(\xi-x)+1)^{-1}\xi^\nu d\xi$ $(\nu > -1)$ is the Fermi–Dirac function.

Taking into account relations (5)–(8), one can write Equations (1) and (2) in dimensionless form as follows:

$$\begin{aligned} &\overline{\mathbf{E}} + \overline{\nabla}\overline{\mu}_1 = \tfrac{1}{\overline{M}_{00}}\overline{\mathbf{j}} + \overline{\alpha}\overline{\nabla}\overline{T},\ \overline{\mathbf{E}} = \mathbf{E}/E_{au},\ E_{au} = E_H/(ea_B),\ \overline{\alpha} = \alpha/e; \\ &\overline{\mathbf{q}} = \left(\tfrac{x\overline{K}_{00} - \overline{K}_{01}/\overline{T}}{x\overline{M}_{00} - \overline{M}_{01}/\overline{T}}\overline{\alpha} - x\right)\overline{T}\overline{\mathbf{j}} - \overline{\kappa}\overline{\nabla}\overline{T}, \overline{\mathbf{q}} = \tfrac{\mathbf{q}}{q_{au}}, q_{au} = \tfrac{{E_H}^2}{\hbar {a_B}^2}, \overline{\kappa} = \tfrac{\kappa}{\kappa_{au}}, \kappa_{au} = \tfrac{E_H}{\hbar a_B}. \end{aligned} \tag{9}$$

The thermoelectric coefficient $\overline{\alpha}$ and electronic thermal conductivity $\overline{\kappa}$ in (9) have the following form:

$$\begin{aligned} \overline{\alpha} &= x - \tfrac{\overline{M}_{01}}{\overline{T}\overline{M}_{00}} = x - \tfrac{\frac{\partial}{\partial x}\int_0^\infty \xi^2\bar{l}_{j,eff}(\xi)f_0(\xi-x)d\xi}{\frac{\partial}{\partial x}\int_0^\infty \xi\bar{l}_{j,eff}(\xi)f_0(\xi-x)d\xi}; \\ \overline{\kappa} &= \tfrac{1}{\overline{T}}\left(\overline{K}_{02} - \tfrac{\overline{M}_{01}\overline{K}_{01}}{\overline{M}_{00}}\right) + x\left(\tfrac{\overline{K}_{00}\overline{M}_{01}}{\overline{M}_{00}} - \overline{K}_{01}\right). \end{aligned} \tag{10}$$

As follows from the relations above, it is necessary to determine the calculation method of the two mean free paths, $\bar{l}_{j,eff}$ and $\bar{l}_{q,eff}$, in order to calculate the transport characteristics of a metal, particularly iron. Here, we will divide the metal in an expanded state ($\delta = V_{a0}/V_a = \rho/\rho_0 < 1$) from the compressed one ($\delta \geq 1$). In the expanded state, both of these mean free paths are equal. In the compressed state, the heat transfer by electrons at temperatures lower than the Debye temperature is more favorable in the transition of electrons from the states above the Fermi surface to the states below it than due to the diffusion along its surface [30,31]. To find the mean free path, similar to [21,22,24], we will use the fundamental relation of the diffraction model of the metal [32], which J. I. Frenkel used in the 1920s to explain the dependence of electrical conductivity on temperature. Its essence is the analogy between the scattering of conduction electrons and light on density fluctuations as follows [33]:

$$l_j^{-1} = \frac{m^2 n_i}{4\pi\hbar^4 k^4}\int_0^{2k} {S_i}^2(q)\left|\langle \mathbf{k}+\mathbf{q}|w_i|\mathbf{k}\rangle\right|^2 \varepsilon(q)^{-2}q^3 dq \tag{11}$$

Here, in (11), $k = (2m\varepsilon_e)^{1/2}/\hbar$ is the wavenumber of the conduction electron with energy ε_e and mass m. ${S_i}^2(q)$ is the square of the ionic static structural factor of metallic plasma (for an ideal gas of ions (atoms) ${S_i}^2(q) = 1$). In the long-wavelength approximation, ${S_i}^2(q)$ is as follows [21,22,24]:

$${S_i}^2(0) = {S_{ii}}^{-1},\ S_{ii} = \frac{K_{ii}(\rho,T)}{n_i T} \tag{12}$$

Here, $K_{ii} = \rho \partial P_i / \partial \rho|_T$ is the modulus of isothermal compressibility of an ionic metal component, $|\langle \mathbf{k} + \mathbf{q} | w_i | \mathbf{k} \rangle|^2$ is the squared form factor of unshielded ions or atoms, $\varepsilon(q) = 1 + k_D{}^2 q^{-2}$ is the static permittivity of the Debye plasma, $k_D{}^2 = \min\{k_s{}^2, k_{ei}{}^2\}$ is the squared Debye wavenumber of plasma, $k_s = r_s{}^{-1}$, $r_s = (3/4\pi n_i)^{1/3}$ is the average interatomic distance, $k_{ei2} = k_{De}{}^2 + (k_{Di}{}^4 + k_s{}^4) k_D{}^{-2}$, $k_{Di}{}^2 = 4\pi e^2 z_i{}^2 n_i{}^2 / T$ is the squared Debye wavenumber of an ion, and $k_{De}{}^2 = 2\pi e^2 z_i n_i F_{-1/2}(\mu_1/T)/F_{1/2}(\mu_1/T)$ is the squared Debye wavenumber of an electron. To find the form factor of an unshielded ion, one has to use the effective potential of an ion as follows [21,22,24]:

$$w_i(r) = -\frac{e^2 z_i}{r} + \frac{e^2 (Z - z_i)}{r} \exp\left(-\frac{r}{r_c}\right), \; r_c = \frac{Z - z_i}{Z^{3/2}} \left(\frac{\langle r^2 \rangle_a}{6}\right)^{1/2} \tag{13}$$

where r_c is the shielding radius of the internal electron, and the values of $\langle r_c \rangle_a$ are averaged over the electronic density of the atom [34]. Similarly to [32], one can obtain the expression for the squared form factor for the case of a spherically symmetric potential (13) as follows:

$$|\langle \mathbf{k} + \mathbf{q} | w_i | \mathbf{k} \rangle|^2 = 16\pi^2 e^4 \left(\frac{z_i{}^2}{q^4} + \frac{(Z - z_i)^2 r_c{}^4}{(1 + q^2 r_c{}^2)^4}\right). \tag{14}$$

It is supposed for expression (14) that the main contribution to the mean free path is defined by the scattering of conduction electrons on the internal electrons of the atom when $z_i << Z$ (see [21,22,24] and the references therein). The contribution of the second term in the potential (13) and its form factor to the mean free path is significant for considering the weakly ionized substance ($z_i << Z$) in the expanded state ($\delta < 1$). The accounting of scattering by an atom's internal electrons in the compressed state requires separate investigations. That is why in this paper, for the first approximation, we will neglect it for simplicity.

It is known [30] that for the compressed state, the cutoff factor is the Debye wavenumber $q_D = (6\pi^2 / V_a)^{1/3} = q_{D0} \delta^{1/3}$ [1]. The structural factor for the compressed state of a metal can be represented as follows [24]:

$$S_i{}^2(q) = S_{ii}{}^{-1} \frac{\frac{q}{q_D}\frac{\Theta}{T}}{\exp\left(\frac{q}{q_D}\frac{\Theta}{T}\right) - 1} = S_{ii}{}^{-1} \frac{\frac{q}{q_D}\frac{\hbar\omega_D}{T}}{\exp\left(\frac{q}{q_D}\frac{\hbar\omega_D}{T}\right) - 1} \tag{15}$$

Here, in (15), $\Theta = \hbar\omega_D$ is the Debye temperature of a metal in a compressed state. It depends on the density (volume of atom cell) [1]. Given the above, we can write the expression for the dimensionless mean free path used in (8)–(10) in the form as follows:

$$\bar{l}_j(\bar{\varepsilon}_e) = \frac{\bar{\varepsilon}_e{}^2 S_{ii}(\bar{n}_i, \overline{T})}{\pi \bar{n}_i \Lambda_j(\langle \bar{\varepsilon}_e \rangle)} \tag{16}$$

where

$$\Lambda_j(\langle \bar{\varepsilon}_e \rangle) = \begin{cases} z_i{}^2 \Lambda_{j,c}(\langle \bar{\varepsilon}_e \rangle) \text{ for } \overline{V}_a \le \overline{V}_{a0} \; (\delta = \overline{V}_{a0}/\overline{V}_a \ge 1); \\ z_i{}^2 \Lambda_{j,ex1}(\langle \bar{\varepsilon}_e \rangle) + (Z - z_i)^2 \Lambda_{j,ex2}(\langle \bar{\varepsilon}_e \rangle) \text{ for } \overline{V}_a > \overline{V}_{a0} \; (\delta < 1). \end{cases} \tag{17}$$

Here, in (17), $\Lambda_{j,c}(\langle \bar{\varepsilon}_e \rangle)$, $\Lambda_{j,ex1}(\langle \bar{\varepsilon}_e \rangle)$, and $\Lambda_{j,ex2}(\langle \bar{\varepsilon}_e \rangle)$ are the analogs of the Coulomb logarithms. They are widely used to describe the transport properties of ideal plasma.

$$\Lambda_{j,c}(\langle \bar{\varepsilon}_e \rangle) = b_1{}^4 \int_0^{(8 < \bar{\varepsilon}_e >)^{1/2} \overline{\omega}_D / \bar{q}_D \overline{T}} \frac{\zeta^4 d\zeta}{(\exp(\zeta) - 1)(1 + b_1{}^2 \zeta^2)^2}, \; b_1 = \frac{\bar{q}_D}{\bar{k}_D} \frac{\overline{T}}{\overline{\omega}_D} \tag{18}$$

$$\Lambda_{j,ex1}(\langle \bar{\varepsilon}_e \rangle) = \int_0^{(8 < \bar{\varepsilon}_e >)^{1/2} / \bar{k}_D} \frac{\zeta^3 d\zeta}{(1 + \zeta^2)^2} \tag{19}$$

$$\Lambda_{j,ex2}(\langle\bar{\varepsilon}_e\rangle) = {b_2}^4 \int_0^{(8<\bar{\varepsilon}_e>)^{1/2}/\bar{k}_D} \frac{\zeta^7 d\zeta}{(1+{b_2}^2\zeta^2)^2(1+\zeta^2)^2},\ b_2 = \bar{r}_c\bar{k}_D \tag{20}$$

To reduce the calculation difficulties of the kinetic coefficients, these integrals in (18)–(20) will be defined with the use of the average energy of the conduction electron. For the case under investigation, this energy is only the function of the temperature and volume of the atomic cell.

Then, the mean free path l_q, which defines the heat transferred by electrons, is given by the following relation:

$$\bar{l}_q(\bar{\varepsilon}_e) = \frac{\bar{\varepsilon}_e{}^2 S_{ii}(\overline{n}_i, \overline{T})}{\pi\overline{n}_i\Lambda_q(\langle\bar{\varepsilon}_e\rangle)} \tag{21}$$

Based on the conclusions made in [24,31], $\Lambda_q(\langle\bar{\varepsilon}_e\rangle)$ can be written as follows:

$$\Lambda_q(\langle\bar{\varepsilon}_e\rangle) = \begin{cases} {z_i}^2\Lambda_{j,c}(\langle\bar{\varepsilon}_e\rangle)\left(1+3\pi^{-2}\left(\bar{k}_F\bar{q}_D{}^{-1}\right)^2\left(\overline{\omega}_D\overline{T}^{-1}\right)^2\right) \text{for } \overline{V}_a \le \overline{V}_{a0}\ (\delta \ge 1); \\ {z_i}^2\Lambda_{j,ex1}(\langle\bar{\varepsilon}_e\rangle) + (Z-z_i)^2\Lambda_{j,ex2}(\langle\bar{\varepsilon}_e\rangle) \text{ for } \overline{V}_a > \overline{V}_{a0}\ (\delta < 1). \end{cases} \tag{22}$$

In (22), $\bar{k}_F = \left(3\pi^2 z_i(\overline{V}_a, \overline{T}=0)/\overline{V}_a\right)^{1/3}$ is the wavenumber of an electron on the Fermi surface. When $\overline{T} \to \overline{\omega}_D$ and $\overline{V}_a \le \overline{V}_{a0}\ (\delta \ge 1)$, it follows from relation (18) that $\Lambda_{j,c} \cong 4!{b_1}^4 = 24(\bar{q}_D\overline{T}/\bar{k}_D\overline{\omega}_D)^4$. The mean free paths have the following asymptotic behavior for this case:

$$\begin{aligned} \bar{l}_j(\bar{\varepsilon}_e) &= \frac{\bar{\varepsilon}_e{}^2 S_{ii}\left(\overline{n}_i,\overline{T}\right)}{\pi\overline{n}_i\Lambda_j(\langle\bar{\varepsilon}_e\rangle)} = \frac{\bar{\varepsilon}_e{}^2 S_{ii}\left(\overline{n}_i,\overline{T}\right)}{24\pi\overline{n}_i{z_i}^2(\bar{q}_D\overline{T}/\bar{k}_D\overline{\omega}_D)^4} \propto \frac{\bar{\varepsilon}_e{}^2}{\overline{n}_i{z_i}^2\overline{T}}\left(\frac{\bar{k}_D\overline{\omega}_D}{\bar{q}_D\overline{T}}\right)^4 \propto \overline{T}^{-5}; \\ \bar{l}_q(\bar{\varepsilon}_e) &= \frac{\bar{\varepsilon}_e{}^2 S_{ii}\left(\overline{n}_i,\overline{T}\right)}{\pi\overline{n}_i\Lambda_j(\langle\bar{\varepsilon}_e\rangle)\left(1+3\pi^{-2}\left(\bar{k}_F\bar{q}_D{}^{-1}\right)^2\left(\overline{\omega}_D\overline{T}^{-1}\right)^2\right)} \cong \frac{\pi\bar{\varepsilon}_e{}^2 S_{ii}\left(\overline{n}_i,\overline{T}\right)\left(\bar{k}_D\overline{\omega}_D\right)^4}{72\overline{n}_i{z_i}^2(\bar{q}_D\overline{T})^2\left(\bar{k}_F\overline{\omega}_D\right)^2} \propto T^{-3}. \end{aligned} \tag{23}$$

The relations obtained above, (16) for $\bar{l}_j(\bar{\varepsilon}_e)$ and (21) for $\bar{l}_q(\bar{\varepsilon}_e)$, along with the Equations (17)–(20) and (22), allow one to calculate the Onsager electronic kinetic coefficient (8). Therefore, it is possible to determine the electrical $\overline{\sigma}(\delta, \overline{T})$ and thermal conductivities $\overline{\kappa}(\delta, \overline{T})$ and thermoelectric coefficient $\overline{\alpha}(\delta, \overline{T})$ in a broad range of densities and temperatures.

First, it is worth discussing the behavior of the shielding parameters of the ions' potential and its internal electrons as functions of the volume of an atomic cell and temperature. Figure 1a shows the behavior of the squared Debye wavenumbers of electrons $\bar{k}_{De}{}^2(\overline{V}_a, \overline{T})$ and ions $\bar{k}_{Di}{}^2(\overline{V}_a, \overline{T})$ and $\bar{k}_D{}^2(\overline{V}_a, \overline{T})$ in comparison with the behavior of the squared mean wavenumbers $\bar{k}_s{}^2 = (3/4\pi\overline{n}_i)^{-2/3}$. The behavior of the squared shielding radius of the inner electrons is shown in Figure 1b.

The left dotted line, which corresponds to the value of $\overline{V}_0 \equiv \overline{V}_{a0} = 79.516$, separates the compressed state from the expanded one. The right dotted line with the value of $\overline{V} = \overline{V}_{MIT} = 457.513$ corresponds to the metal–insulator PT boundary. In this case, the overlap of the electron wave functions disappears at zero temperature, i.e., the electrons appear to be localized. This value of the volume in atomic units corresponds to the values of the relative and real density of iron: $\delta_{MIT} = 0.174$, $\rho_{MIT} = 1.368$, g/cm^3. The iron parameters corresponding to this critical point were obtained earlier [1]: $\overline{V} = \overline{V}_{cr} = 302.348$, $\delta_{cr} = 0.263$, $\rho_{cr} = 2.07$, g/cm^3. The comparison of curves in Figure 1a shows that the Debye screening radius of the ion potential coincides with $\bar{r}_s$. The curves in Figure 1b show that $\bar{r}_c{}^2$ is practically independent of the temperature up to the critical one. A further increase in the temperature leads to its decrease, which is used to associate with an ionization increase, i.e., a decrease in the number of internal electrons of the ions.

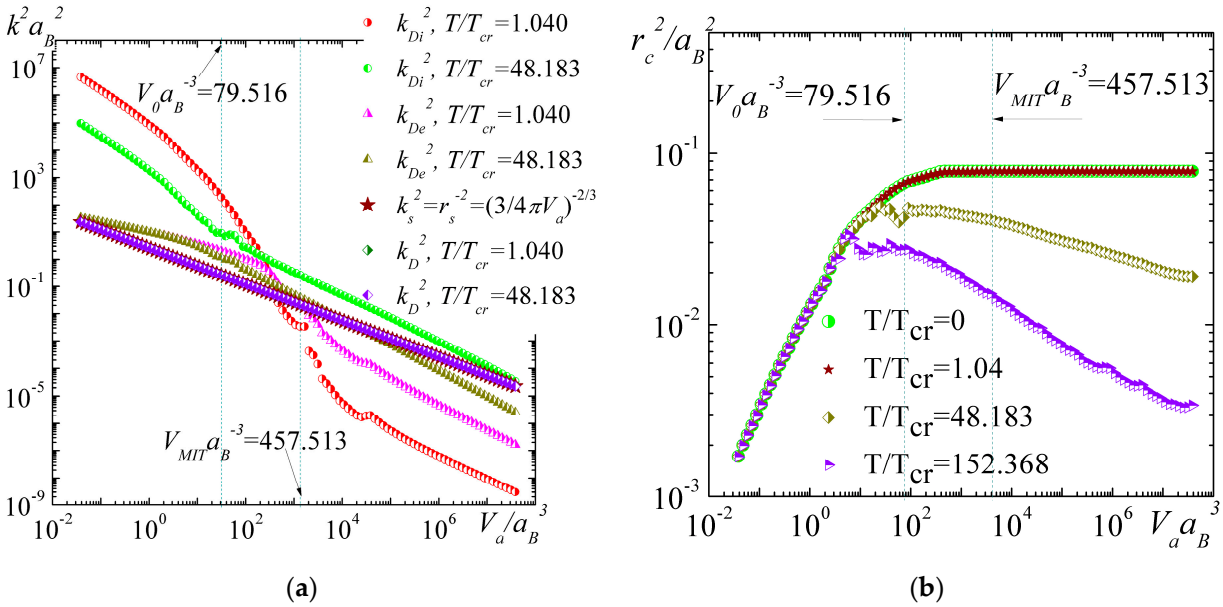

Figure 1. The squared Debye wavenumbers (**a**) and the squared shielding radius of inner electrons (**b**).

Figure 2 shows the behavior of the long-wavelength structure factor $S_{ii}(\delta,T)$ of iron in dependence on δ for low (a) and high (b) temperatures. As above, the dotted line in Figure 2a,b corresponds to the relative critical density δ_{cr} = 0.263. An analysis of the curves shows that the figure plotted on a logarithmic scale cannot contain points with a negative value of the structure factor $S_{ii}(\delta,T)$. Strictly speaking, the presence of these negative values shows the limitation of the hydrodynamic approximation in the liquid–gas PT range. It is possible to use the hydrodynamic approximation when the mean free is limited by the following condition: $\bar{l}_j \geq \bar{r}_s$.

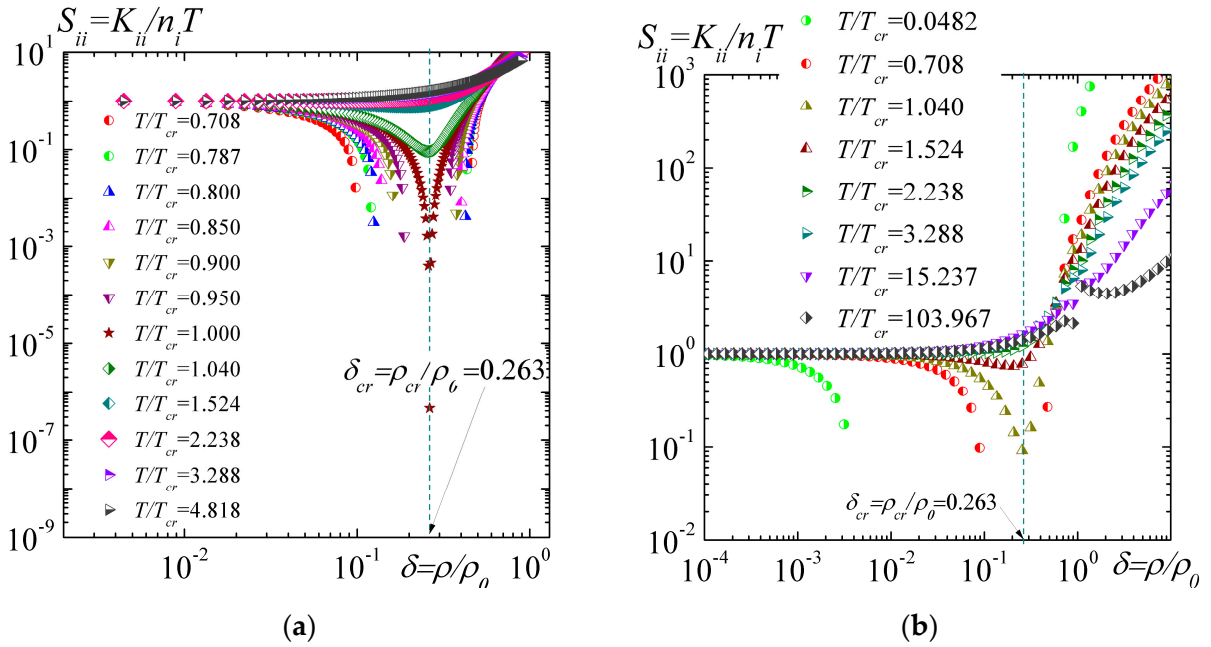

Figure 2. The long-wavelength structure factor of iron for low (**a**) and high temperatures (**b**).

The following modification of expression (8) is proposed for calculating the Onsager coefficients $\overline{M}_{0\beta}$ for $\overline{V}_a > \overline{V}_{a0} (\delta < 1)$:

$$\overline{M}_{0\beta} = \frac{\sqrt{2} z_i \overline{n}_i \overline{T}^{\beta-1/2}}{3} \frac{\frac{\partial}{\partial x} \int_0^\infty \xi^{\beta+1} \overline{l}_{j,eff}(\xi) f_0(\xi - x) d\xi}{F_{1/2}(x)} =$$

$$= \begin{cases} \frac{\sqrt{2} z_i \overline{T}^{\beta+3/2}}{3\pi\Lambda_j(\langle\overline{\varepsilon}_e\rangle)} \frac{\frac{\partial}{\partial x} \int_0^\infty \xi^{\beta+3} f_0(\xi - x) d\xi}{F_{1/2}(x)} = \frac{\sqrt{2} z_i \overline{T}^{\beta+3/2}}{3\pi\Lambda_j(\langle\overline{\varepsilon}_e\rangle)} \frac{F'_{\beta+3}(x)}{F_{1/2}(x)} \text{ for } S_{ii} > 0; \\ \frac{\sqrt{2} z_i \overline{n}_i \overline{r}_s \overline{T}^{\beta-1/2}}{3} \frac{\frac{\partial}{\partial x} \int_0^\infty \xi^{\beta+1} f_0(\xi - x) d\xi}{F_{1/2}(x)} = \frac{\sqrt{2} z_i \overline{n}_i \overline{r}_s \overline{T}^{\beta-1/2}}{3} \frac{F'_{\beta+1}(x)}{F_{1/2}(x)} \text{ for } S_{ii} \leq 0. \end{cases} \quad (24)$$

The expressions for the electrical conductivity, thermal conductivity, and thermoelectric coefficient will be the following for the case $\overline{V}_a > \overline{V}_{a0} (\delta < 1)$:

$$\overline{\sigma} = \overline{M}_{00} = \begin{cases} \frac{\sqrt{2} z_i \overline{T}^{3/2}}{3\pi\Lambda_j(\langle\overline{\varepsilon}_e\rangle)} \frac{F'_3(x)}{F_{1/2}(x)} = \frac{\sqrt{2} z_i \overline{T}^{3/2}}{\pi\Lambda_j(\langle\overline{\varepsilon}_e\rangle)} \frac{F_2(x)}{F_{1/2}(x)} \text{ for } S_{ii} > 0; \\ \frac{\sqrt{2} z_i \overline{n}_i \overline{r}_s}{3\overline{T}^{1/2}} \frac{F'_1(x)}{F_{1/2}(x)} = \frac{\sqrt{2} z_i \overline{n}_i \overline{r}_s}{3\overline{T}^{1/2}} \frac{F_0(x)}{F_{1/2}(x)} \text{ for } S_{ii} \leq 0. \end{cases} \quad (25)$$

$$\overline{\kappa} = \begin{cases} \frac{\sqrt{2} z_i \overline{T}^{5/2} S_{ii}}{3\pi\Lambda_j(\langle\overline{\varepsilon}_e\rangle)} \left(\frac{F'_5(x)}{F_{1/2}(x)} - \frac{(F'_4(x))^2}{F'_3(x) F_{1/2}(x)} \right) = \\ = \frac{5\sqrt{2} z_i \overline{T}^{5/2} S_{ii}}{3\pi\Lambda_j(\langle\overline{\varepsilon}_e\rangle)} \left(\frac{F_4(x)}{F_{1/2}(x)} - \frac{16}{15} \frac{{F_3}^2(x)}{F_2(x) F_{1/2}(x)} \right) \text{ for } S_{ii} > 0; \\ \frac{\sqrt{2} z_i \overline{n}_i \overline{r}_s \overline{T}^{1/2}}{3} \left(\frac{F'_3(x)}{F_{1/2}(x)} - \frac{(F'_2(x))^2}{F'_1(x) F_{1/2}(x)} \right) = \\ = \sqrt{2} z_i \overline{n}_i \overline{r}_s \overline{T}^{1/2} \left(\frac{F_2(x)}{F_{1/2}(x)} - \frac{4}{3} \frac{{F_1}^2(x)}{F_0(x) F_{1/2}(x)} \right) \text{ for } S_{ii} \leq 0. \end{cases} \quad (26)$$

$$\overline{\alpha} = \begin{cases} x - \frac{F_4'(x)}{F_3'(x)} = x - \frac{4}{3} \frac{F_3(x)}{F_2(x)} \text{ for } S_{ii} > 0; \\ x - \frac{F_2'(x)}{F_1'(x)} = x - \frac{2F_1(x)}{F_0(x)} \text{ for } S_{ii} \leq 0. \end{cases} \quad (27)$$

Expressions (25)–(27), along with the expressions for σ, κ, and α for a metal in the compressed state, and the Wiedemann–Franz law $\overline{\kappa}/\overline{\sigma} = L_{WF}\overline{T}$, (here, L_{WF} is Lorenz number [35]) make it possible to calculate these values in a broad range of densities and temperatures.

The dotted line shows the critical density in Figures 3a and 4a. The density of the metal–insulator PT at $T = 0$ is marked by such a line in Figure 3b. The value of $T/T_{cr} = 1$ is shown with a dashed line in Figure 5a,b. As one can see, the electrical conductivity is proportional to the number of electrons in an atomic cell in the area of weakly ionized metallic plasma. It is in complete agreement with the theory of weakly ionized ideal gases [28,36].

On the basis of the data analysis shown in Figures 3–6, one can conclude that the behaviors of the electrical conductivity, thermal conductivity, and thermoelectric coefficient give the correct theoretical asymptotes. As expected, the largest variation of these values is observed near the critical point.

A detailed comparison of the electrical conductivity near the critical point with the experimental results [37,38] is considered in Section 3 below.

2.2. Optical Properties of Metal Irradiated by Pulsed Radiation from a Solid-State Laser

The electric field of a laser pulse incident along the normal to a metal surface can be expressed as $E = E_0(t)\exp(-i\omega_0 t)$, where $\omega_0 = c{\lambda_L}^{-1}$ is its frequency, λ_L is the wavelength of the laser radiation, and E_0 is the envelope of the laser pulse amplitude that changes slowly in comparison with its frequency ω_0. We used a pulsed Q-switched Nd:YAG solid-state LOTIS TII LS-2134D laser for the experiments [39,40]. This laser could produce the radiation of the first and second harmonics with wavelengths of $\lambda_{L1} = 1064$ nm ($\omega_{L1} = 2.82 \times 10^{14}$, s^{-1}) and $\lambda_{L2} = 532$ nm ($\omega_{L2} = 5.64 \times 10^{14}$, s^{-1}), respectively. Here and below, the index "*L1*" means the first harmonic of laser radiation, and "*L2*" means the second one.

To determine the plasma's optical characteristics, we assumed that the plasma is uniform and isotropic and that the electric field intensity $E(\omega)$ is low.

In this case, the distribution function of electrons can be expressed as $f = f_0 + \mathbf{v}_e \cdot \mathbf{f}_1/v_e = f_0 + \mathbf{p} \cdot \mathbf{f}_1/p$, where $\mathbf{v}_e \cdot \mathbf{f}_1/v_e << f_0$ (here, $\mathbf{v}_e$ and $\mathbf{p}$ are the velocity and momentum). Due to the high laser frequencies, the symmetric function does not explicitly depend on the time since it depends on the temperature and ion concentration. The change in the last ones is determined by the slow hydrodynamic processes. Hence, $f_0 = (\exp((\varepsilon_e - \mu_1)/T) + 1)^{-1}$ is the equilibrium Fermi–Dirac function we used both in [1] and in the previous section. Then, in the approximation we used for solving the Boltzmann equation, the expression for the asymmetric term of the distribution function of electrons in a periodic electric field takes the following form:

$$\mathbf{f}_1(\omega) = -\frac{ev_e \frac{\partial f_0}{\partial \varepsilon_e}}{-i\omega + \nu_{ei}(\varepsilon_e)}\mathbf{E}(\omega) = \frac{e\left(\frac{2\varepsilon_e}{m}\right)^{1/2}\frac{\partial f_0}{\partial \mu_1}}{-i\omega + (2\varepsilon_e/m)^{1/2} l_{j,eff}{}^{-1}(\varepsilon_e)}\mathbf{E}(\omega) \quad (28)$$

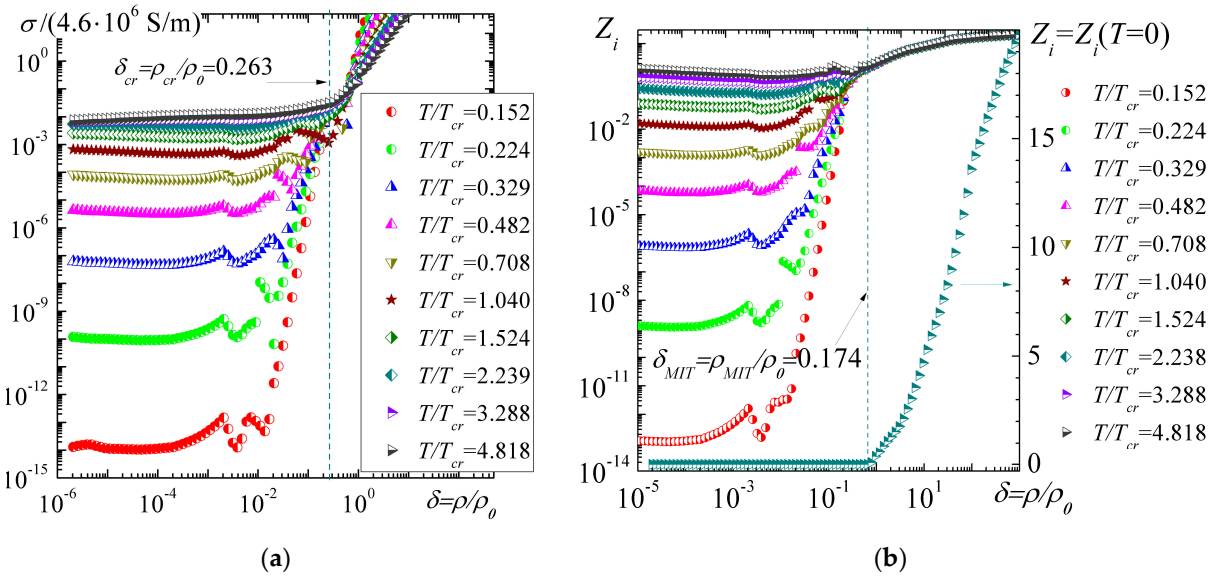

Figure 3. The electron conductivity (**a**) and number of electrons in an atomic cell (**b**) of iron.

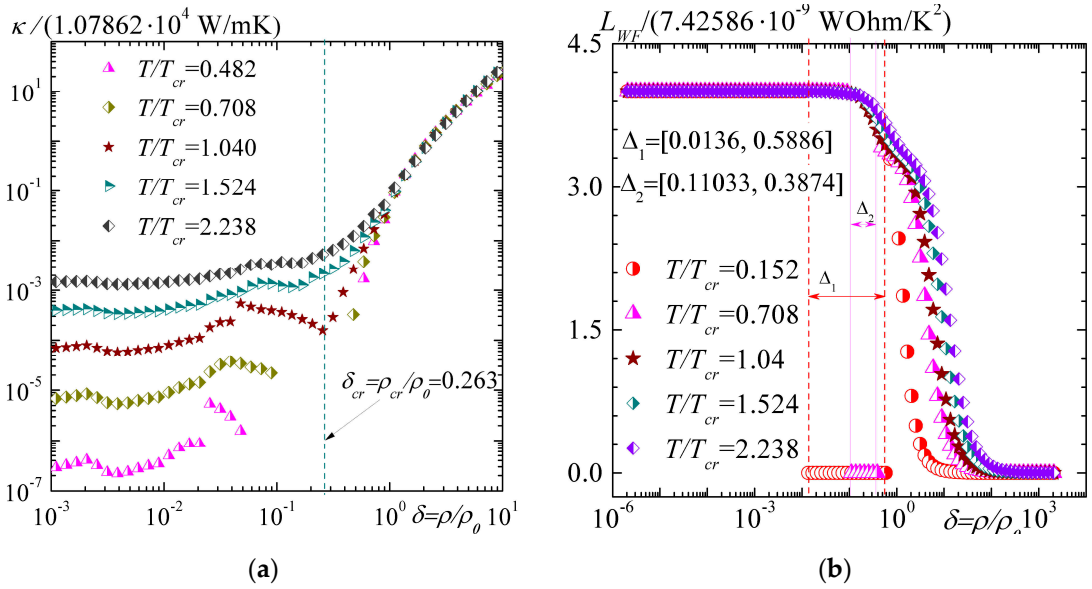

Figure 4. The dependence of iron thermal conductivity (**a**) and Wiedemann–Franz ratio (**b**) on density.

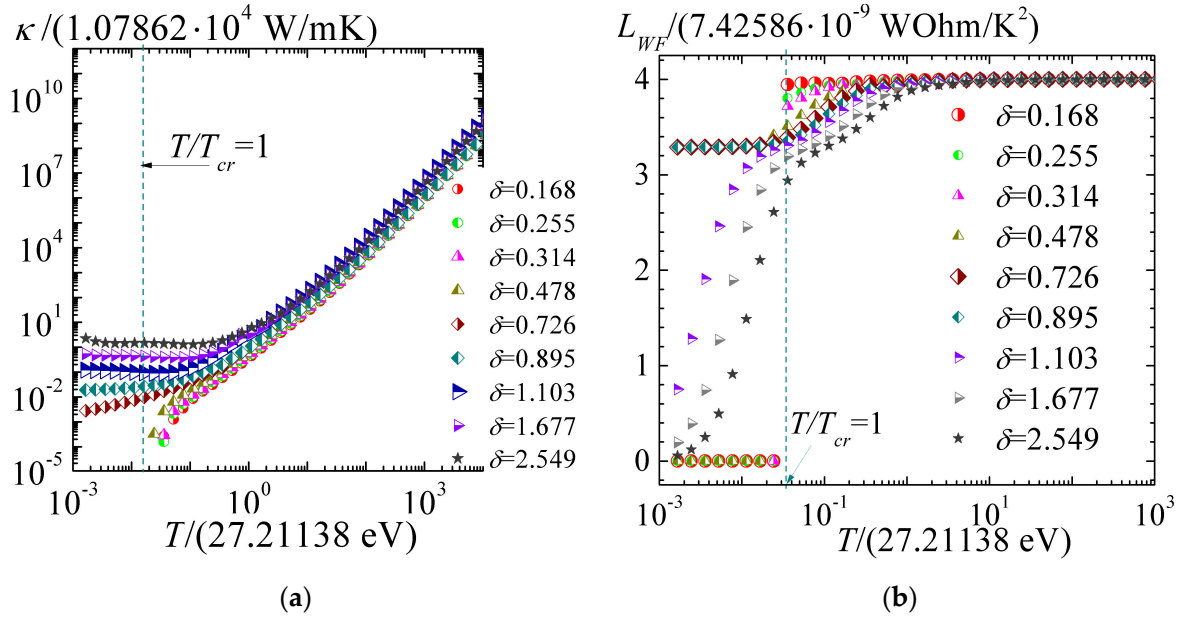

Figure 5. The dependence of iron thermal conductivity (**a**) and Wiedemann–Franz ratio (**b**) on temperature.

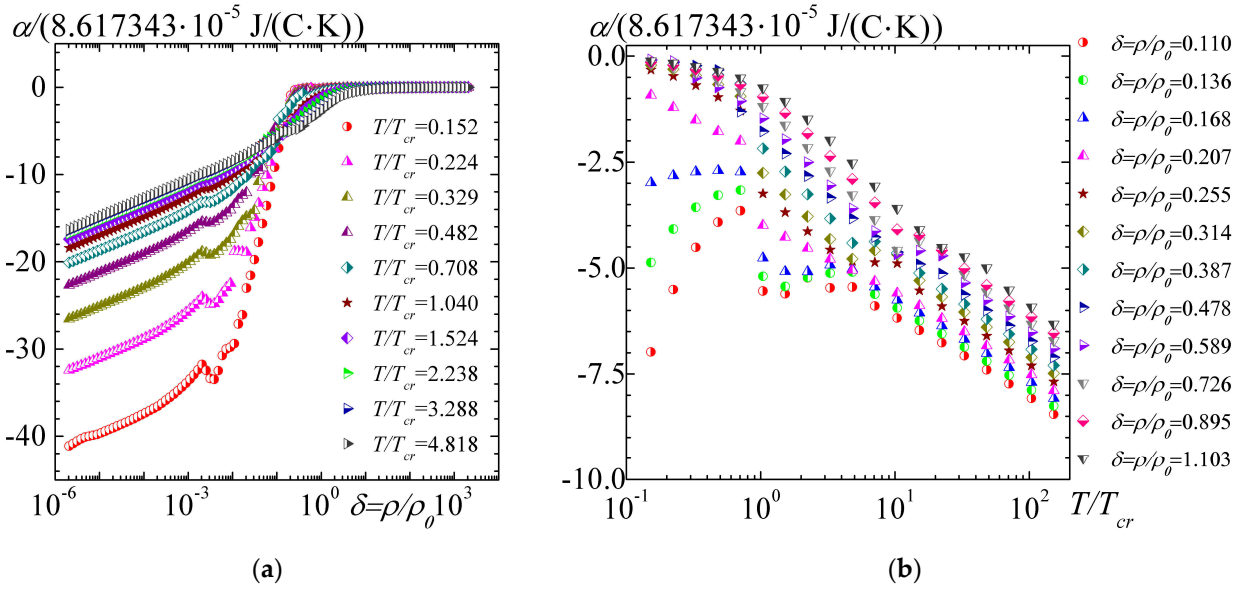

Figure 6. The dependence of thermoelectric coefficient on density (**a**) and temperature (**b**).

In (28), $l_{j,eff}(\varepsilon_e)$ is the free path of an electron. The technique used to determine this value was discussed in the previous section as follows:

$$\mathbf{j}' = 2e\int \mathbf{v}_e f \frac{d^3\mathbf{p}}{(2\pi\hbar)^3} = \frac{(2m)^{3/2}e^2}{3m\pi^2\hbar^3}\frac{\partial}{\partial\mu_1}\int_0^\infty \frac{{\varepsilon_e}^{3/2}f_0 d\varepsilon_e}{-i\omega+\nu_{ei}(\varepsilon_e)}\mathbf{E} = \frac{2z_i n_i e^2}{3m}\frac{\frac{\partial}{\partial\mu_1}\int_0^\infty \frac{{\varepsilon_e}^{3/2}f_0 d\varepsilon_e}{-i\omega+\nu_{ei}(\varepsilon_e)}}{\int_0^\infty {\varepsilon_e}^{1/2}f_0 d\varepsilon_e}\mathbf{E} =$$

$$= \left(\frac{2z_i n_i e^2}{3m}\frac{\frac{\partial}{\partial\mu_1}\int_0^\infty \frac{\nu_{ei}(\varepsilon_e){\varepsilon_e}^{3/2}f_0 d\varepsilon_e}{\omega^2+{\nu_{ei}}^2(\varepsilon_e)}}{\int_0^\infty {\varepsilon_e}^{1/2}f_0 d\varepsilon_e} + i\omega\frac{2z_i n_i e^2}{3m}\frac{\frac{\partial}{\partial\mu_1}\int_0^\infty \frac{{\varepsilon_e}^{3/2}f_0 d\varepsilon_e}{\omega^2+{\nu_{ei}}^2(\varepsilon_e)}}{\int_0^\infty {\varepsilon_e}^{1/2}f_0 d\varepsilon_e}\right)\mathbf{E} =$$

$$= -i\omega\frac{\varepsilon'(\omega)-1}{4\pi}\mathbf{E} = -i\omega\frac{\varepsilon_1(\omega)-1+i\varepsilon_2(\omega)}{4\pi}\mathbf{E}.$$

Then, one can obtain the following expressions for the real and imaginary parts of the complex permittivity:

$$\varepsilon_1(\omega) = 1 - \frac{2{\omega_p}^2}{3}\frac{\frac{\partial}{\partial\mu_1}\int_0^\infty \frac{{\varepsilon_e}^{3/2} f_0 d\varepsilon_e}{\omega^2 + {\nu_{ei}}^2(\varepsilon_e)}}{\int_0^\infty {\varepsilon_e}^{1/2} f_0 d\varepsilon_e} = 1 - \frac{2{\overline{\omega}_p}^2}{3}\frac{\frac{\partial}{\partial x}\int_0^\infty \frac{\xi^{3/2} f_0(\xi - x)d\xi}{\overline{\omega}^2 + {\overline{\nu}_{ei}}^2(\xi)}}{F_{1/2}(x)} \tag{29}$$

$$\varepsilon_2(\omega) = \frac{2{\omega_p}^2}{3\omega}\frac{\frac{\partial}{\partial\mu_1}\int_0^\infty \frac{\nu_{ei}(\varepsilon_e){\varepsilon_e}^{3/2} f_0 d\varepsilon_e}{\omega^2 + {\nu_{ei}}^2(\varepsilon_e)}}{\int_0^\infty {\varepsilon_e}^{1/2} f_0 d\varepsilon_e} = \frac{2{\overline{\omega}_p}^2}{3\overline{\omega}}\frac{\frac{\partial}{\partial x}\int_0^\infty \frac{\overline{\nu}_{ei}(\xi)\xi^{3/2} f_0(\xi - x)d\xi}{\overline{\omega}^2 + {\overline{\nu}_{ei}}^2(\xi)}}{F_{1/2}(x)} \tag{30}$$

In (29) and (30), $\omega_p = \left(4\pi z_i n_i e^2/m\right)^{1/2} = \omega_{au}\overline{\omega}_p$, $\overline{\omega}_p = \left(4\pi z_i n_i e^2/m\right)^{1/2}{\omega_{au}}^{-1}$ is the frequency of plasma oscillations of electrons, and $\omega_{\text{au}} = E_{\text{h}}/\hbar$ is the basic frequency in the SAU (see Appendix A). The high-frequency ($\overline{\omega} >> \overline{\nu}_{ei}$) asymptotic of $\varepsilon_{1,HF}(\overline{\omega})$ follows from relation (29). It does not depend on the statistics of electrons as follows [25]:

$$\varepsilon_{1,HF}(\omega) = 1 - \frac{2{\overline{\omega}_p}^2}{3\overline{\omega}^2}\frac{\frac{\partial}{\partial x}\int_0^\infty \xi^{3/2} f_0(\xi - x)d\xi}{F_{1/2}(x)} = 1 - \frac{2{\overline{\omega}_p}^2}{3\overline{\omega}^2}\frac{F'_{3/2}(x)}{F_{1/2}(x)} = 1 - \frac{2{\overline{\omega}_p}^2}{3\overline{\omega}^2}\frac{3F_{1/2}(x)}{2F_{1/2}(x)} = 1 - \frac{{\overline{\omega}_p}^2}{\overline{\omega}^2}$$

Expressions (29) and (30) in an equivalent form for the laser frequency $\overline{\omega}_L = \omega_L/\omega_{au}$ will be the following:

$$\begin{aligned} &\varepsilon_1(\overline{\omega}_L) = 1 - \frac{2{\overline{\omega}_p}^2}{3{\overline{\omega}_L}^2}\frac{J_{11}(x) - J_{12}(x)}{F_{1/2}(x)}, \\ &J_{11}(x) = \int_0^\infty \frac{{\overline{\omega}_L}^2\xi^{3/2}d\xi}{(\exp(\xi - x) + 1)({\overline{\omega}_L}^2 + {\overline{\nu}_{ei}}^2(\xi))}, J_{12}(x) = \int_0^\infty \frac{{\overline{\omega}_L}^2\xi^{3/2}d\xi}{(\exp(\xi - x) + 1)^2({\overline{\omega}_L}^2 + {\overline{\nu}_{ei}}^2(\xi))}; \end{aligned} \tag{31}$$

$$\begin{aligned} &\varepsilon_2(\overline{\omega}_L) = \frac{2{\overline{\omega}_p}^2}{3{\overline{\omega}_L}^2}\frac{J_{21}(x) - J_{22}(x)}{F_{1/2}(x)}, \\ &J_{21}(x) = \int_0^\infty \frac{\overline{\omega}_L\overline{\nu}_{ei}(\xi)\xi^{3/2}d\xi}{(\exp(\xi - x) + 1)({\overline{\omega}_L}^2 + {\overline{\nu}_{ei}}^2(\xi))}, J_{22}(x) = \int_0^\infty \frac{\overline{\omega}_L\overline{\nu}_{ei}(\xi)\xi^{3/2}d\xi}{(\exp(\xi - x) + 1)^2({\overline{\omega}_L}^2 + {\overline{\nu}_{ei}}^2(\xi))}. \end{aligned} \tag{32}$$

To calculate the integrals $J_{11}(x)$, $J_{12}(x)$, $J_{21}(x)$, and $J_{22}(x)$, one can use the method analogous to the one used for the calculation of the kinetic coefficients $\overline{M}_{0\beta}$ in the region $\delta < 1$ (see (24)). Then, the expressions for these integrals will be as follows:

$$J_{11}(x) = \begin{cases} {A_1}^2\int_0^\infty \frac{\xi^{9/2}d\xi}{(\exp(\xi - x) + 1)(1 + {A_1}^2\xi^3)}, A_1 = \frac{S_{ii}\overline{\omega}_L\overline{T}^{3/2}}{\sqrt{2}\pi\overline{n}_i\Lambda_j}, S_{ii} > 0 \\ \int_0^\infty \frac{\xi^{3/2}d\xi}{(\exp(\xi - x) + 1)(1 + {A_2}^2\xi)}, A_2 = \frac{\sqrt{2\overline{T}}}{\overline{\omega}_L\overline{r}_s}, S_{ii} \le 0 \end{cases}, \tag{33}$$

$$J_{12}(x) = \begin{cases} {A_1}^2\int_0^\infty \frac{\xi^{9/2}d\xi}{(\exp(\xi - x) + 1)^2(1 + {A_1}^2\xi^3)}, A_1 = \frac{S_{ii}\overline{\omega}_L\overline{T}^{3/2}}{\sqrt{2}\pi\overline{n}_i\Lambda_j}, S_{ii} > 0 \\ \int_0^\infty \frac{\xi^{3/2}d\xi}{(\exp(\xi - x) + 1)^2(1 + {A_2}^2\xi)}, A_2 = \frac{\sqrt{2\overline{T}}}{\overline{\omega}_L\overline{r}_s}, S_{ii} \le 0 \end{cases}, \tag{34}$$

$$J_{21}(x) = \begin{cases} A_1\int_0^\infty \frac{\xi^3 d\xi}{(\exp(\xi - x) + 1)(1 + {A_1}^2\xi^3)}, A_1 = \frac{S_{ii}\overline{\omega}_L\overline{T}^{3/2}}{\sqrt{2}\pi\overline{n}_i\Lambda_j}, S_{ii} > 0 \\ A_2\int_0^\infty \frac{\xi^2 d\xi}{(\exp(\xi - x) + 1)(1 + {A_2}^2\xi)}, A_2 = \frac{\sqrt{2\overline{T}}}{\overline{\omega}_L\overline{r}_s}, S_{ii} \le 0 \end{cases}, \tag{35}$$

$$J_{22}(x) = \begin{cases} A_1\int_0^\infty \frac{\xi^3 d\xi}{(\exp(\xi - x) + 1)^2(1 + {A_1}^2\xi^3)}, A_1 = \frac{S_{ii}\overline{\omega}_L\overline{T}^{3/2}}{\sqrt{2}\pi\overline{n}_i\Lambda_j}, S_{ii} > 0; \\ A_2\int_0^\infty \frac{\xi^2 d\xi}{(\exp(\xi - x) + 1)^2(1 + {A_2}^2\xi)}, A_2 = \frac{\sqrt{2\overline{T}}}{\overline{\omega}_L\overline{r}_s}, S_{ii} \le 0. \end{cases} \tag{36}$$

If a laser electromagnetic wave propagates to a dispersive non-magnetic medium, then one can consider it to be a monochromatic plane wave with a complex wavenumber $k_L = \sqrt{\varepsilon'}\omega_L/c = (n_L + i\kappa_L)\omega_L/c$ [41]. Here, $n_L = n(\omega_L)$ is the refractive index, and $\kappa_L = \kappa(\omega_L)$ is the absorption coefficient of the medium. If we square the wavenumber, we can obtain

the following expressions: ${n_L}^2 - {\kappa_L}^2 = \varepsilon_1(\omega_L)$, $2n_L\kappa_L = \varepsilon_2(\omega_L)$. Then, the expressions for n_L and κ_L will be as follows:

$$n_L = \sqrt{\frac{\varepsilon_1 + \sqrt{{\varepsilon_1}^2 + {\varepsilon_2}^2}}{2}}, \kappa_L = \sqrt{\frac{-\varepsilon_1 + \sqrt{{\varepsilon_1}^2 + {\varepsilon_2}^2}}{2}} \quad (37)$$

The solution of the one-dimensional Helmholtz equation gives the spatial distribution of the envelope of the electric field of the laser pulse as follows:

$$\frac{\partial^2 E(z,\omega_L)}{\partial z^2} + \frac{\left(({n_L}^2 - {\kappa_L}^2) + i2n_L\kappa_L\right){\omega_L}^2}{c^2} E(z,\omega_L) = 0 \quad (38)$$

The change in the internal energy of the plasma due to laser heating depends at least on the plasma density and temperature. It can be expressed as follows [42,43]:

$$Q_L(t,z) = I_L(t)\beta_L|E(t,z)/E_L(t)|^2 = I_L(t)\beta_L \exp\left(-\int_z^\infty \beta_L(z')dz'\right) \quad (39)$$

Here, $I_L(t)$ is the laser radiation intensity, and $\beta_L = {a_B}^{-1}\overline{\beta}_L = {a_B}^{-1}\varepsilon_2(\overline{\omega}_L)\overline{\omega}_L/\overline{c}$ is the dimensional absorption coefficient of the laser radiation, with the dimension m^{-1} in SI. Expressions (31)–(36) and (39) make it possible to calculate all the optical characteristics of the metal in a broad range of densities and temperatures.

The obtained data presented in Figures 7–11 allow one to conclude that plasma is transparent for optical radiation at a low density and weak ionization. Thus, for $T/T_{cr} = 0.048$, the real part of the permittivity becomes negative when passing from $\delta = 0.168$ to $\delta = 0.207$. It indicates the quasi-free conduction electrons' appearance (see Figures 7a and 9a). The density value of $\delta_{MIT} = 0.174$ corresponding to the metal–insulator PT at $T = 0$, i.e., the localization of electrons, was calculated using the LmtART ver. 7 software (https://savrasov.physics.ucdavis.edu) [9,10].

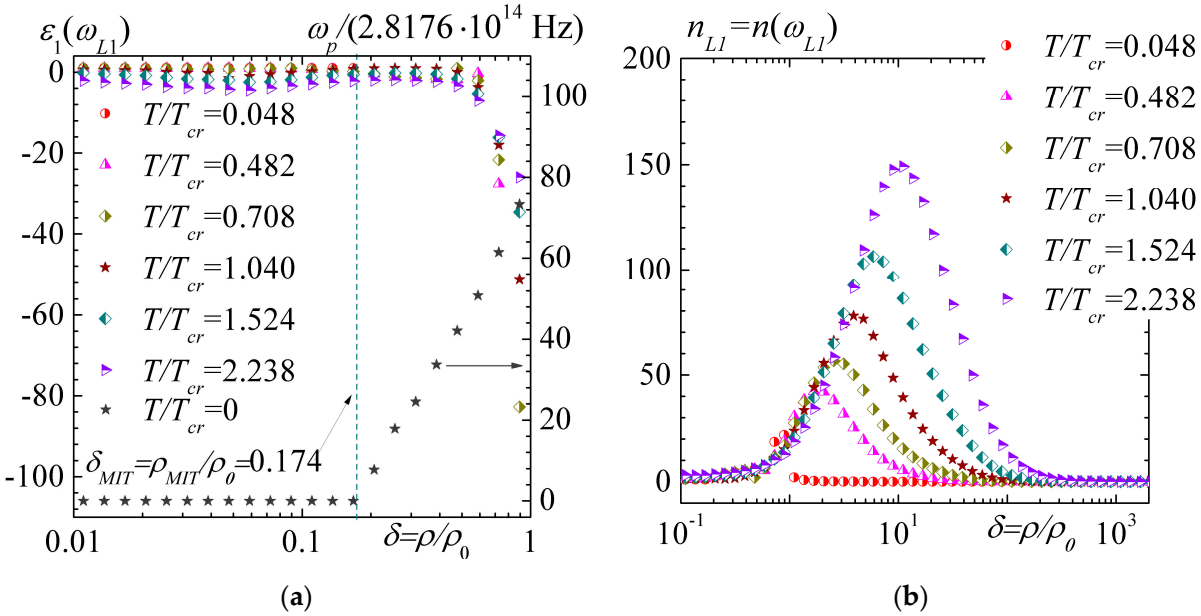

Figure 7. The real permittivity (**a**) and refraction index (**b**) of iron for the first harmonic of laser radiation.

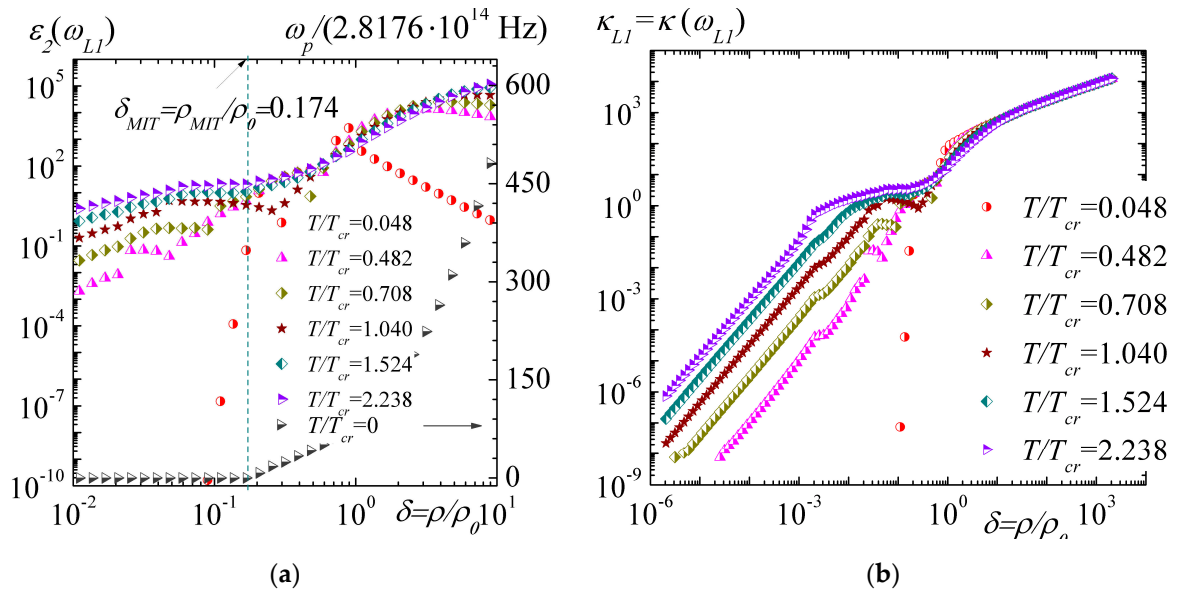

Figure 8. The imaginary permittivity (**a**) and absorption factor (**b**) of iron for the first harmonic of laser radiation.

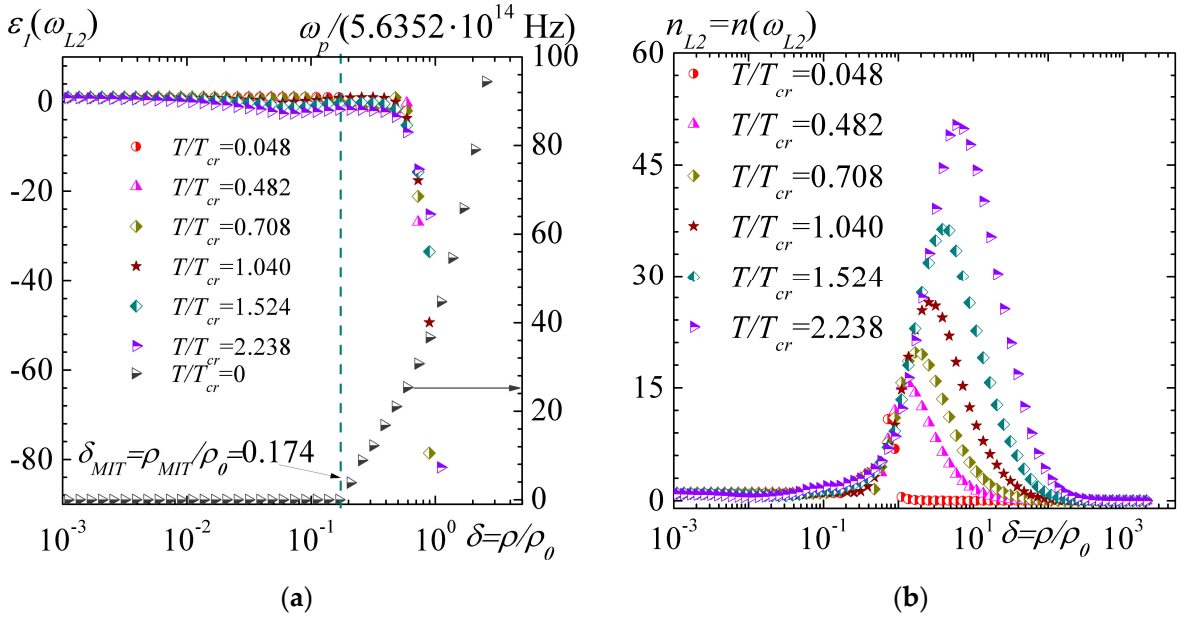

Figure 9. The real permittivity (**a**) and refraction index (**b**) of iron for the second harmonic of laser radiation.

The greatest absorption is observed in the region of the compressed state of the metal. One can see it in Figures 8b, 10b and 11. The maximum change in the transport and optical properties of iron is observed near the liquid–gas PT in the area of critical density and in the area of density corresponding to the metal–insulator PT at $T = 0$.

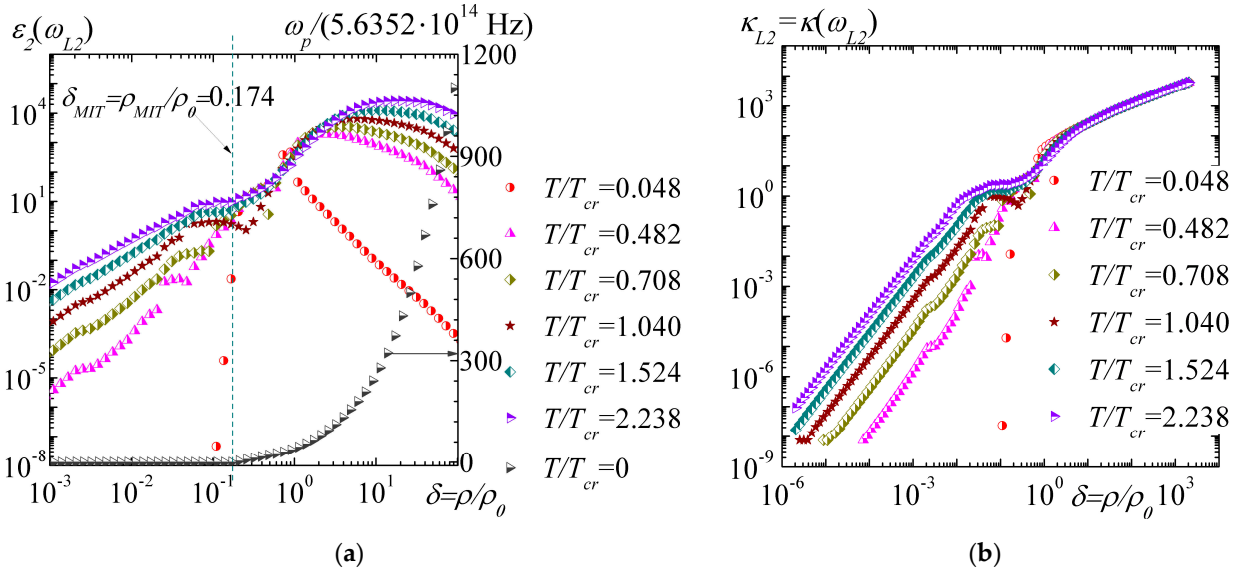

Figure 10. The imaginary permittivity (**a**) and absorption factor (**b**) of iron for the second harmonic of laser radiation.

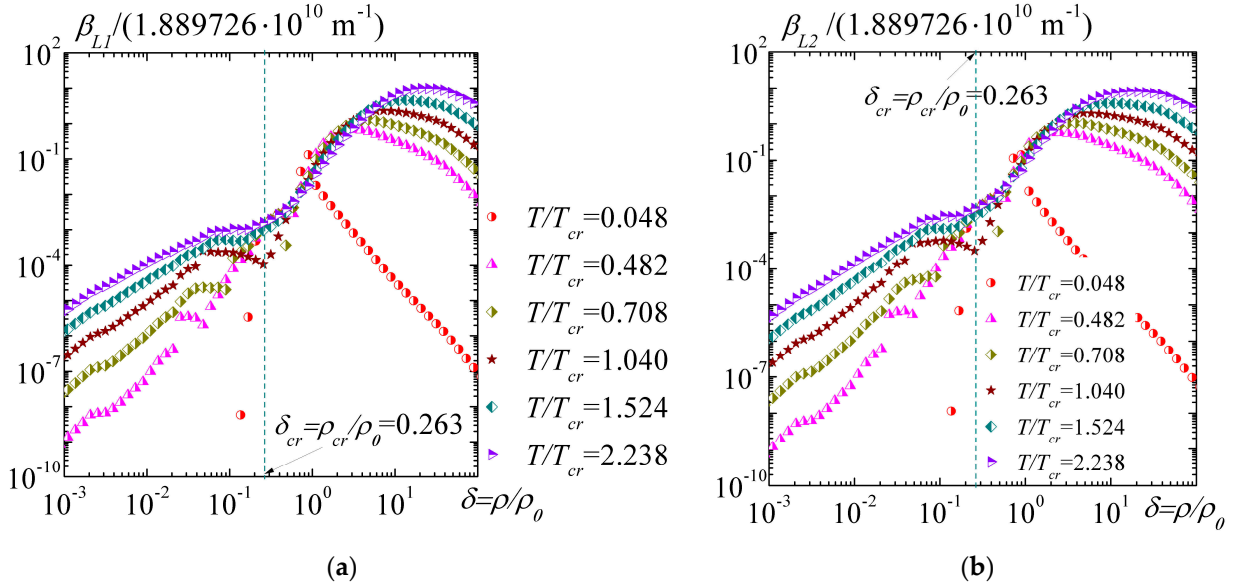

Figure 11. The absorption coefficient of iron for the first (**a**) and the second (**b**) harmonics of laser radiation.

3. Discussion

Figure 12 demonstrates the behavior of the calculated electrical conductivity of iron as a function of temperature (Figure 12a) and density (Figure 12b).

The dependences of the dimensionless absorption coefficient on the matter density for the first and second laser radiation harmonics are shown in Figure 13.

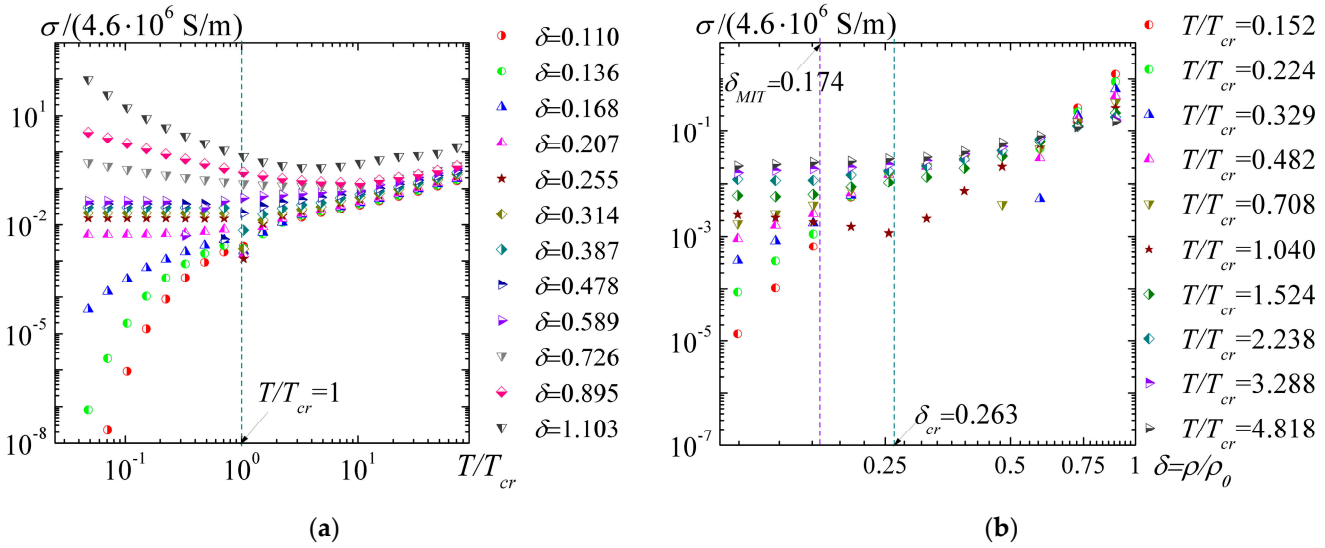

Figure 12. The dependence of electronic conductivity of iron on temperature (**a**) and density (**b**).

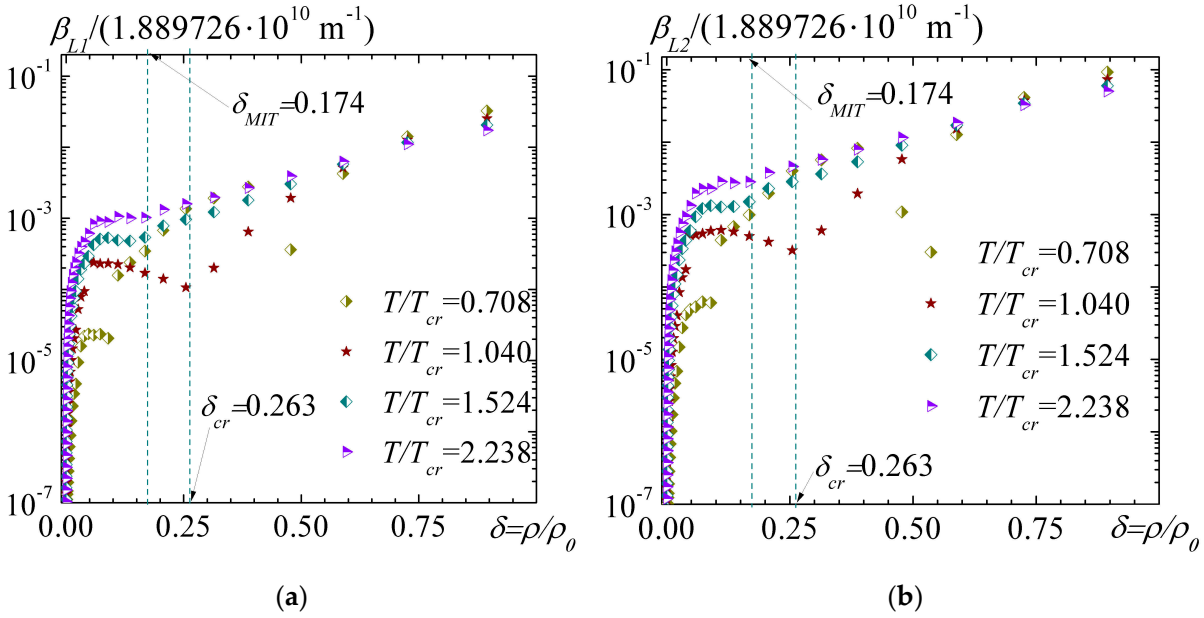

Figure 13. The dimensionless iron absorption coefficient for the first (**a**) and second (**b**) harmonics of the laser radiation.

The change in the electrical conductivity character from a metallic type to a non-metallic one in the range of relative volume V/V_0 = 3–5 (relative density δ = 0.2–0.33) for pressures P = 20–25 kbar was shown in recently published experimental investigations [37,38]. According to these papers, the presence of a metal–insulator PT is shown to be near the critical point of the liquid–gas PT, which was predicted in [44]. Thus, it seems reasonable to compare our results with the experimental data of these papers. It should be taken into account that the estimates of the critical parameters of iron used in [37,38] to interpret these experiments were the following: ρ_{cr} = 2.03 g/cm^3, T_{cr} = 9600 K, and P_{cr} = 8.25 kbar [45]. But we will use the following parameters of the critical point of iron, which we obtained from [1]: ρ_{cr} = 2.07 g/cm^3, T_{cr} = 10867 K, and P_{cr} = 12.56 kbar. The experimental pressure range of P = 20–25 kbar corresponds to P_{exp}/P_{cr} = 2.424–3.03 in [37,38] and P_{exp}/P_{cr} = 1.59–1.99 in our paper [1]. The change in the electrical conductivity character was observed experimentally in the range V/V_0 = 3–5. This range in Figure 12a corresponds to three isodensities (isochores): (1) δ = 0.21 (V/V_0 = 4.84), (2) δ = 0.26 (V/V_0 = 3.92),

and (3) $\delta = 0.31$ ($V/V_0 = 3.18$). The first value corresponds to the change in resistivity: $T/T_{cr} = 0.71$ $\rho_e = 29.03$ μΩ·m, $T/T_c = 1.04$ $\rho_e = 141.77$ μΩ·m, $T/T_c = 1.52$ $\rho_e = 24.96$ μΩ·m. The second value corresponds to $T/T_c = 0.71$ $\rho_e = 14.51$ μΩ·m, $T/T_c = 1.04$ $\rho_e = 186.89$ μΩ·m, $T/T_c = 1.52$ $\rho_e = 20.57$ μΩ·m. The third value corresponds to $T/T_c = 0.71$ $\rho_e = 10.33$ μΩ·m, $T/T_c = 1.04$ $\rho_e = 99.38$ μΩ·m, $T/T_c = 1.52$ $\rho_e = 16.21$ μΩ·m. These results agree with the data shown in Figures 12b and 13a,b. The last two figures show that at $\delta = 0.263$ ($V/V_0 = 3.802$), the absorption coefficient of the laser radiation energy decreases sharply. This behavior of the resistivity and energy absorption coefficient of laser radiation in the near-critical region of the liquid–gas PT is explained by the behavior of the structural factor $S_{ii} = K_{ii}/n_iT$, which is responsible for the density fluctuations in the near-critical and supercritical areas (see Figure 2a, as well as [46]). It should be noted that the curves in Figure 12a, corresponding to the density below the PT at $T = 0$ ($\delta = 0.110$–0.168), demonstrate the plasma behavior with the increasing temperature. The curves corresponding to the density range $\delta = 0.726$–1.103 show a uniform change in the electrical conductivity from a metallic character to a plasma one with a temperature increase.

4. Conclusions

In Section 2.1, on the example of iron, the expressions of the following transport properties of a matter in the expanded and compressed state were obtained: electrical conductivity $\sigma(\rho,T)$, electronic thermal conductivity $\kappa(\rho,T)$, and thermoelectric coefficient $\alpha(\rho,T)$. These expressions were used to calculate the above-mentioned parameters in a broad range of densities and temperatures. In Section 2.2, the expressions for the real and imaginary parts of the permittivity and the absorption coefficient laser radiation were obtained. The analysis of these characteristics in the expanded and compressed states was carried out. They appear to be consistent with the known results in limiting cases.

The impurity additions to an ordered medium are widely used for theoretical studies of the metal–insulator PT. These impurities violate the original order [7,47–50]. Then, we can consider two limiting cases. The first case corresponds to the white noise when the correlation radius between the impurities is zero. The second corresponds impurity to the infinite correlation radius [7]. The case of $S_{ii}(\delta,T) = 1$ corresponds to the first limiting case of uncorrelated impurities in the commonly developed theoretical models of the metal–insulator PT. The process descriptions we use in the near-critical region, $S_{ii}(\delta,T) \neq 1$ and $\delta < 1$, are closer to the second limiting case, supposing an infinite correlation radius. Therefore, the properties and structural PTs of metals in the expanded and compressed states are the aims of further studies.

Thus, it was established that the behaviors of the transport and optical characteristics in the near-critical and supercritical regions of iron in the liquid state do not contradict the experimental data [37,38], and the proposed model can be applied to the estimation of metal properties in compressed and expanded states under the influence of high-density energy fluxes.

Author Contributions: Conceptualization, N.B.V.; investigation, A.I.L. All authors have read and agreed to the published version of the manuscript.

Funding: This research was funded by the Russian Science Foundation and the Government of Sverdlovsk Region, project no. 22-29-20058.

Data Availability Statement: The data that support the findings of this study are available upon reasonable request from the authors.

Acknowledgments: We are grateful to S.Y. Savrasov for giving us the opportunity to use the LmtART-7 software package for the calculation of the electronic spectra of iron in the framework of the density functional theory.

Conflicts of Interest: The authors declare no conflict of interest.

Appendix A

Table A1 contains brief information about the system of atomic units (SAU). We hope it will simplify the understanding of the text of the article. The values of the fundamental constants were taken from the handbook in [29]. The derived physical constants (Bohr radius and below) in Table A1 were specially calculated to adapt their values to the expressions in the main text and to simplify the reproduction of our calculations if needed.

Table A1. Brief information about some physical quantities in the system of atomic units.

Unit Symbol and Definition	SGS	SI
Light velocity: c	$2.99792458 \times 10^{10}$ cm/s	2.99792458×10^{8} m/s
Boltzmann constant: k_B	$1.3806505 \times 10^{-16}$ erg/K	$1.3806505 \times 10^{-23}$ J/K
Reduced Planck constant: $\hbar$	$1.05457168 \times 10^{-27}$ erg·s	$1.05457168 \times 10^{-27}$ J·s
Electron mass: m	$9.1093826 \times 10^{-28}$ g	$9.1093826 \times 10^{-31}$ kg
Electron rest energy: $E_0 = mc^2$	$8.187104787 \times 10^{-7}$ erg	$8.187104787 \times 10^{-14}$ J
Fine structure constant: α_{FSC}	$7.297352568 \times 10^{-3}$	$7.297352568 \times 10^{-3}$
Elementary charge: e	$4.80332044 \times 10^{-10}$ GSG	$1.60217653 \times 10^{-19}$ C
Basic energy: $E_H = {\alpha_{FSC}}^2 \cdot E_0$	$4.3597442 \times 10^{-11}$ erg	$4.3597442 \times 10^{-18}$ J
Bohr radius: a_B	$5.2917721 \times 10^{-11}$ cm	5.2917721×10^{-9} m
Wavenumber: $q_B = {a_B}^{-1}$	$1.889726142 \times 10^{8}$ cm^{-1}	$1.889726142 \times 10^{10}$ m^{-1}
Basic square: $S_{au} = {a_B}^2$	2.8×10^{-17} cm^2	2.8×10^{-21} m^2
Basic volume: $V_{au} = {a_B}^3$	1.481847×10^{-25} cm^3	1.481847×10^{-31} m^3
Particle concentration: $N = 1/V_{au}$	$6.748334685 \times 10^{24}$ cm^{-3}	$6.748334685 \times 10^{30}$ m^{-3}
Basic time: $t_{au} = \hbar/E_H$	$2.4188843 \times 10^{-17}$ s	$2.4188843 \times 10^{-17}$ s
Basic frequency: $\omega_{\mathrm{au}} = {t_{au}}^{-1}$	$4.134137372 \times 10^{16}$ s^{-1}	$4.134137372 \times 10^{16}$ s^{-1}
Basic velocity: $v_{au} = \alpha_{FSC} \cdot c$	$2.187691263 \times 10^{8}$ cm/s	$2.187691263 \times 10^{6}$ m/s
Basic force: $Fau = E_H/a_B$	$8.238722577 \times 10^{-3}$ dyn	$8.238722577 \times 10^{-8}$ N
Basic pressure: $Pau = E_H/V_{au}$	294.2101296 Mbar	29.42101296 TPa
Basic current: $I_{au} = ev_{au}/a_B$	$1.985710681 \times 10^{7}$ SGS	$6.6236178688 \times 10^{-3}$ A
Basic voltage: $U_{au} = E_H/e$	0.09076741 SGS	27.211384712 V
Electric strength: $E_{au} = E_H/e \cdot a_B$	$1.715255461 \times 10^{7}$ SGS	$5.142206506 \times 10^{11}$ V/m
Current density: $J_{\mathrm{au}} = I_{au}/S_{au}$	$7.091101703 \times 10^{23}$ SGS/cm^2	$2.365336324 \times 10^{18}$ A/m^2
Electric conductivity: $\sigma_{au} = J_{au}/E_{au}$	$4.134137372 \times 10^{16}$ s^{-1}	4.5998482×10^{6} S/m
Thermal conductivity: $\kappa_{en} = 1/(a_B \cdot t_{au})$	$7.812387468 \times 10^{24}$ (cm·s)$^{-1}$	$7.812387468 \times 10^{26}$ (m·s)$^{-1}$
$\kappa_{au} = \kappa_{en} \cdot k_B$	1.07861767×10^{9} erg/(s·cm·K)	1.07861767×10^{4} W/(m·K)
Thermal power: $\alpha_{au} = k_B/e$	$2.87443628 \times 10^{-7}$ erg/(K·SGS)	$8.61734318 \times 10^{-5}$ J/(C·K)

References

1. Volkov, N.B.; Lipchak, A.I. Thermodynamic functions of a metal exposed to high energy densities in composed and expanded states. *Condens. Matter* **2022**, *7*, 61. [CrossRef]
2. Maxwell, J.C. On the Dynamical Theory of Gases. In *Scientific Papers of James Clark Maxwell*, 2nd ed.; Two Volumes Bound As One; Niven, W.D., Ed.; Dover Publications, Inc.: Mineola, NY, USA, 1965; Volume 2, pp. 26–78.
3. Boltzmann, L. *Lectures on Gas Theory*; Stephen, G. Brush, S.G., Translator; Dover Publications, Inc.: Mineola, NY, USA, 1995.
4. Lorentz, H.A. *The Theory of Electrons: Its Applications to the Phenomena of Light and Radiant Heat (Dover Books on Physics)*, 2nd ed.; Dover Publications, Inc.: Mineola, NY, USA, 2011.
5. Abrikosov, A.A.; Gorkov, L.P.; Dzyaloshinskii, I.E. *Methods of Quantum Field Theory in Statistical Physics*; Pergamon Press Ltd.: Oxford, UK, 1963.
6. Mahan, G.D. *Many-Particle Physics*, 3rd ed.; Kluwer Academic/Plenum Publishers: New York, NY, USA, 2000.

7. Sadovskii, M.V. *Diagrammatics: Lectures on Selected Problems in Condensed Matter Theory*; World Scientific Publishing Co. Pte. LTD: Singapore, 2006.
8. Mahan, G.D. Quantum transport equation for electric and magnetic fields. *Phys. Rep.* **1987**, *145*, 251–318. [CrossRef]
9. Savrasov, S.Y. Linear-response theory and lattice dynamics: A muffin-orbital approach. *Phys. Rev. B* **1996**, *54*, 16470–16486. [CrossRef] [PubMed]
10. Savrasov, S.Y.; Savrasov, D.Y. Electron-phonon interactions and related physical properties of metals from linear-response theory. *Phys. Rev. B* **1996**, *54*, 16487–16501. [CrossRef] [PubMed]
11. Maksimov, E.G.; Savrasov, D.Y.; Savrasov, S.Y. The electron–phonon interaction and the physical properties of metals. *Physics-Uspekhi* **1997**, *40*, 337–358. [CrossRef]
12. Giustino, F. Electron–phonon interactions from first principles. *Rev. Mod. Phys.* **2017**, *89*, 015003. [CrossRef]
13. Ichimaru, S. Strongly coupled plasmas: High-density classical plasmas and degenerate electron liquids. *Rev. Mod. Phys.* **1982**, *54*, 1017–1059. [CrossRef]
14. Kraeft, W.-D.; Kremp, D.; Ebeling, W.; Roepke, G. *Quantum Statistics of Charged Particle Systems*; Akademy-Verlag: Berlin, Germany, 1986.
15. Ebeling, W.; Foerster, A.; Fortov, V.E.; Gryaznov, V.K.; Polishchuk, A.Y. *Thermophysical Properties of Hot Dense Plasmas*; B.G. Teubner Verlagsgeselschaft: Stuttgart, Germany, 1991.
16. Ebeling, W.; Fortov, V.E.; Filinov, V.S. *Quantum Statistics of Dense Gases and Nonideal Plasmas*; Springer Int. Publishing AG: Berlin/Heidelberg, Germany, 2017.
17. Fortov, V.E.; Filinov, V.S.; Larkin, A.S.; Ebeling, W. *Statistical Physics of Dense Gases and Nonideal Plasmas*; Fizmatlit: Moscow, Russia, 2020.
18. Povarnitsyn, M.E.; Knyazev, D.V.; Levashov, P.R. Ab initio simulation of complex dielectric function for dense aluminum plasma. *Contrib. Plasma Phys.* **2012**, *52*, 145–148. [CrossRef]
19. Knyazev, D.V.; Levashov, P.R. Ab initio calculation of transport and optical properties of aluminum: Influence of simulation parameters. *Comput. Mater. Sci.* **2013**, *79*, 817–829. [CrossRef]
20. Knyazev, D.V.; Levashov, P.R. Transport and optical properties of warm dense aluminum in two-temperature regime: Ab initio calculation and semi-empirical approximation. *Phys. Plasmas* **2014**, *21*, 073302. [CrossRef]
21. Volkov, N.B.; Chingina, E.A.; Yalovets, A.P. Dynamical equations and transport coefficients for the metals at high pulse electromagnetic fields. *J. Phys. Conf. Ser.* **2016**, *774*, 012147. [CrossRef]
22. Volkov, N.B.; Nemirovsky, A.Z. The ionic composition of the non-ideal plasma produced by a metallic sphere isothermally expanding into vacuum. *J. Phys. D Appl. Phys.* **1991**, *24*, 693–701. [CrossRef]
23. Shabanskii, V.P. Transfer processes in conductors with regard to nonlinear effects. *Sov. Phys. JETP* **1957**, *4*, 497–508.
24. Volkov, N.B. Nonlinear Dynamics of Current-Carrying Plasma-Like Media. Habilitation Thesis, Institute of Electrophysics UB RAS, Ekaterinburg, Russia, 1999.
25. Ginzburg, V.L. *The Propagation of Electromagnetic Waves in Plasmas*, 2nd ed.; Pergamon Press LTD: Oxford, UK, 1970.
26. Volkov, N.B. A plasma model of the conductivity of metals. *Zhurnal Tekhnicheskoj Fiz.* **1979**, *49*, 2000–2002.
27. Landau, L.D.; Lifshitz, E.M. Statistical Physics, Part 1. In *Course of Theoretical Physics*, 3rd ed.; Pergamon Press LTD: Oxford, UK, 1980; Volume 5.
28. Lifshitz, E.M.; Pitaevskii, L.P. Physical Kinetics. In *Landau and Lifshitz: Course of Theoretical Physics*; Pergamon Press LTD.: Oxford, UK, 1981; Volume 10.
29. Martienssen, W.; Warlimont, H. (Eds.) *Springer Handbook of Condensed Matter and Materials Data*; Springer: Berlin/ Heidelberg, Germany, 2005.
30. Ziman, J.M. *Principles of the Theory of Solids*, 2nd ed.; Cambridge University Press: London, UK, 1972.
31. Berman, R. *Thermal Conduction in Solids*, 2nd ed.; Oxford University Press: Oxford, UK, 1980.
32. Harrison, W.A. *Pseudopotentials in the Theory of Metals*; W. A. Benjamin, INC: New York, NY, USA, 1966.
33. Frenkel, J.I. *Wave Mechanics: Elementary Theory*, 2nd ed.; Dover Publications, INC: Mineola, NY, USA, 1950; Chapter 6.
34. Radtsig, A.A.; Smirnov, B.M. *Reference Book on Atomic and Molecular Physics*; Atomizdat: Moscow, Russia, 1980.
35. Kittel, C. *Introduction to Solid State Physics*, 8th ed.; John Wiley and Sons, Inc.: New York, NY, USA, 2005.
36. Chapman, S.; Cowling, T.G. *The Mathematical Theory of Non-Uniform Gases*, 3rd ed.; Cambridge University Press: Cambridge, UK, 1991.
37. Landau, L.D.; Lifshitz, E.M. Electrodynamics of Continuous Media. In *Course of Theoretical Physics*, 2nd ed.; Pergamon Press LTD: Oxford, UK, 1984; Volume 8.
38. Afanasiev, Y.V.; Krokhin, O.N. High-temperature and plasma phenomena arising from the interaction of high-power laser radiation with matter. In *Physics of High Energy Densities*; International School of Physics "Enrico Fermi" Course, 48; Caldirola, P., Knoepfel, H., Eds.; Academic Press: New York, NY, USA, 1971; Chapter 10.
39. Hora, H. *Physics of Laser Driven Plasma*; John Wiley and Sons, Inc.: New York, NY, USA, 1981.
40. Korobenko, V.N.; Rakhel, A.D. Transition of expanded liquid iron to the nonmetallic state under supercritical pressure. *J. Exp. Theor. Phys.* **2011**, *112*, 649–655. [CrossRef]
41. Korobenko, V.N.; Rakhel, A.D. Observation of a first-order metal-to-nonmetal phase transition in fluid iron. *Phys. Rev. B* **2012**, *85*, 014208. [CrossRef]

42. Lipchak, A.I.; Barakhvostov, S.V. An investigation of the stability of turning a high-current pulse accelerator on with an optical control. *Instrum. Exp. Tech.* **2021**, *64*, 376–380. [CrossRef]
43. Lipchak, A.I.; Barakhvostov, S.V.; Volkov, N.B.; Chingina, E.A.; Turmyshev, I.S. The study of instabilities role of plasma in the high-voltage discharge formation initiated by optical radiation at high pressures in high-voltage optical triggered switches. *J. Phys. Conf. Series* **2021**, *2064*, 012098. [CrossRef]
44. Zeldovich, Y.B.; Landau, L.D. On the relationship between the liquid and gaseous states of metals. *Zh. Exp. Teor. Fiz.* **1944**, *14*, 32.
45. Fortov, V.E.; Iakubov, I.T. *Non-Ideal Plasma*; Pergamon Press LTD: New York, NY, USA, 2000.
46. Brazhkin, V.V. Phase transformations in liquids and the liquid-gas transition in fluids at supercritical pressures. *Phys.-Uspekhi* **2017**, *60*, 954–957. [CrossRef]
47. Mott, N.V. *Metal-Insulator Transitions*; Taylor and Fransis Ltd.: London, UK, 1974.
48. Ziman, J.M. *Models of Disorder*; Cambridge University Press: Cambridge, UK, 1979.
49. Lifshits, I.M.; Gredeskul, S.A.; Pastur, L.A. *Introduction to the Theory of Disorder Systems*; John Wiley and Sons, Inc.: New York, NY, USA, 1988.
50. Gantmakher, V.F. Electrons and Disorder in Solids. In *International Series of Monographs on Physics*; Oxford University Press: Oxford, UK, 2005; Volume 130.